Evolution and morphology of microenvironment-enhanced malignancy of three-dimensional invasive solid tumors

Yang Jiao*
Physical Science in Oncology Center, Princeton University, Princeton, New Jersey 08544, USA

Salvatore Torquato†
Department of Chemistry, Princeton University, Princeton, New Jersey 08544, USA,
Department of Physics, Princeton University, Princeton, New Jersey 08544, USA,
Physical Science in Oncology Center, Princeton University, Princeton, New Jersey 08544, USA, and
Program in Applied and Computational Mathematics, Princeton University, Princeton, New Jersey 08544, USA
(Received 20 December 2012; revised manuscript received 13 March 2013; published 13 May 2013)

The emergence of invasive and metastatic behavior in malignant tumors can often lead to fatal outcomes for patients. The collective malignant tumor behavior resulting from the complex tumor-host interactions and the interactions between the tumor cells is currently poorly understood. In this paper, we employ a cellular automaton (CA) model to investigate microenvironment-enhanced malignant behaviors and morphologies of *in vitro* avascular invasive solid tumors in three dimensions. Our CA model incorporates a variety of microscopic-scale tumor-host interactions, including the degradation of the extracellular matrix by the malignant cells, nutrient-driven cell migration, pressure buildup due to the deformation of the microenvironment by the growing tumor, and its effect on the local tumor-host interface stability. Moreover, the effects of cell-cell adhesion on tumor growth are explicitly taken into account. Specifically, we find that while strong cell-cell adhesion can suppress the invasive behavior of the tumors growing in soft microenvironments, cancer malignancy can be significantly enhanced by harsh microenvironmental conditions, such as exposure to high pressure levels. We infer from the simulation results a qualitative phase diagram that characterizes the expected malignant behavior of invasive solid tumors in terms of two competing malignancy effects: the rigidity of the microenvironment and cell-cell adhesion. This diagram exhibits phase transitions between noninvasive and invasive behaviors. We also discuss the implications of our results for the diagnosis, prognosis, and treatment of malignant tumors.

DOI: 10.1103/PhysRevE.87.052707 PACS number(s): 87.19.lx, 46.32.+x, 87.17.Pq

I. INTRODUCTION

An important problem in cancer biology is the determination of the complex tumor-host and tumor cell-cell interactions and how such interactions lead to various emergent behaviors of malignant tumors, e.g., invasion and metastasis [1]. Specifically, malignant cells can detach from the primary tumor and invade the surrounding tissue. Metastasis occurs when these invasive cells enter the circulation system and reside in other organs to develop secondary tumors. The invasive cells are difficult to remove by resection and often become drug resistant during the chemotherapy that follows surgical removal of the primary tumor. The emergence of invasive and metastatic behaviors in cancer is life threatening. Therefore, significant effort has been expended to understand the mechanisms involved in the invasive growth of malignant tumors [2–9] and their treatment [10,11]. It is generally accepted that the invasive behavior of cancer involves multiple processes including homotype detachment, enzymatic matrix degradation, integrin-mediated heterotype adhesion, and active, directed, and random motility [3,12]. The morphology of a typical invasive tumor is characterized by the dendritic invading branches composed of chains of tumor cells that are emanating from the primary tumor mass [see Fig. 1(a)].

The host microenvironment of a tumor can exert selective forces that dramatically affect tumor morphology and phenotypic evolution and even trigger and enhance invasive behavior [7,8,13,14]. When growing in a confined space such as the cranium, a solid tumor compresses the surrounding microenvironment, which in turn exerts mechanical stresses on the tumor. It has been shown that such confining pressures can significantly affect the growth dynamics of the tumor [15–18]. For example, a tumor growing in a rigid microenvironment (i.e., under a high pressure exerted by the deformed microenvironment) can develop a bumpy surface [see Fig. 1(b)] [19,20]. The invasive cells at the tips of the protrusions on the surface have fewer neighboring cells than those on the smooth tumor surface, which results in weaker cell-cell adhesion. Although the detachment of an invasive cell from the primary tumor is a complex process that involves simultaneously cell-cell signaling and rearrangement of the adhesion structures on the cell surface, it is reasonable to assume that, on average, the cells with fewer neighbors (weaker cell-cell adhesion) find it easier to detach from the primary tumor and migrate into the surrounding microenvironment.

Theoretical and computational cancer modeling that integrates different mechanisms for neoplasm progression, when appropriately linked with experimental and clinical data, offers a promising avenue for a better understanding of tumor evolution [21–25]. Although a variety of mathematical models have been devised for proliferative tumors [26–41], models for invasive tumors incorporating the aforementioned tumor-host

*yjiao@princeton.edu
†torquato@electron.princeton.edu

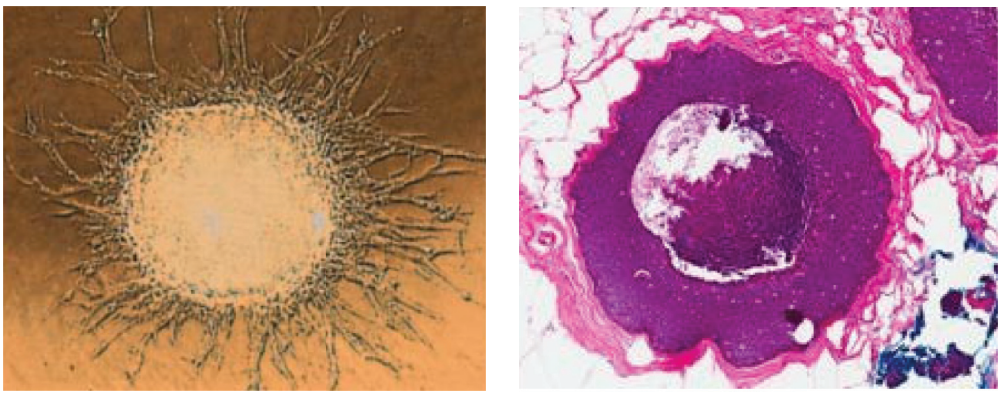

(a) (b)

FIG. 1. (Color online) (a) Dendritic invasive branches composed of chains of tumor cells emanating from the primary tumor mass observed in an assay of glioblastoma multiforme (GBM), the most malignant brain cancer. The image is adapted from Ref. [13]. (b) Emergence of the rough surface on a solid tumor (ductal carcinoma *in situ*), which might lead to further invasive behavior. The image (courtesy of Robert A. Gatenby) is adapted from Ref. [14] (copyright 2012 AIP Advances, licensed under Creative Commons Attribution 3.0 unported).

and tumor cell-cell interactions are rare [7–9,42–45]. Recently, we have developed a cellular automaton (CA) model that enables one to efficiently simulate invasive tumor growth in confined heterogeneous host microenvironment [13,14]. By taking into account a variety of microscopic-scale tumor-host interactions, including the degradation of the extracellular matrix (ECM) by the malignant cells, nutrient-driven cell migration, pressure buildup due to the compression of the microenvironment by the growing tumor, and its effect on the local tumor-host interface stability, our CA model predicts a rich spectrum of morphology, growth dynamics, and emergent behaviors of avascular invasive tumors in *two dimensions*. Specifically, our CA model has successfully reproduced certain salient features of invasive growth including the emergence of dendritic invasive branches emanating from the primary tumor [13] and the development of fingerlike protrusions on the surface of the tumor growing in a rigid microenvironment [14].

In this paper, we further generalize our two-dimensional (2D) model to investigate microenvironment-enhanced malignant behavior of *in vitro* avascular invasive tumors in *three dimensions*. The three-dimensional (3D) model in principle enables one to obtain realistic morphologies of both the primary tumor and invasive branches, which are crucial to the diagnosis, prognosis, and treatment of the tumor. Besides incorporating the aforementioned various tumor-host interactions, the present 3D model also explicitly accounts for the effect of cell-cell adhesion on tumor growth, which is considered to be the primary mechanism ruling the growth dynamics and morphology of the tumors in our study. We note that other mechanisms, such as the accumulation of malignant mutations due to the selective forces induced by the harsh microenvironment, have been modeled to investigate microenvironment-enhanced invasiveness [7,8]. However, we do not consider these mechanisms in our current model.

We find that the invasive behavior of the tumors growing in a soft microenvironment that maintain a smooth and compact shape during the growth process can be suppressed by strong cell-cell adhesion. In contrast, tumors growing in a rigid microenvironment develop fingerlike protrusions on their surfaces. The invasive cells at the tips of such protrusions have a smaller number of neighboring cells and thus they can easily detach from the primary tumor due to the resulting weaker cell-cell adhesion. In other words, the malignant behavior of the tumor is enhanced by the harsh microenvironment condition, i.e., the exposure to high pressure levels. We infer a qualitative phase diagram for possible tumor-malignancy behaviors from our simulation results, which incorporates the aforementioned two competing effects, i.e., microenvironment rigidity and cell-cell adhesion. We show that there are phase transitions between noninvasive and invasive behaviors of a solid tumor, which are induced by increasing the microenvironment rigidity.

The rest of the paper is organized as follows. In Sec. II, we discuss the biophysical background of our computational model and provide the detailed cellular automaton rules. In Sec. III, we employ our CA model to investigate both proliferative and invasive growth of avascular tumors in different microenvironments and propose a phase diagram for malignant tumors based on the simulation results. In Sec. IV, we provide concluding remarks and discuss the implications of our results for cancer diagnosis, prognosis, and therapy.

II. COMPUTATIONAL MODEL

Following Refs. [13] and [14], we use the Voronoi tessellation associated with random-sequential-addition sphere packings [46] to represent the tumor cells and host microenvironment in three dimensions. Specifically, nonoverlapping spheres are randomly and sequentially placed in a prescribed region (i.e., a cubic simulation box) in three-dimensional Euclidean space until there is no void space left for additional spheres. Then the simulation box is divided into polyhedra, each associated with a sphere center, such that any point within a polyhedron (i.e., a Voronoi polyhedron) is closer to its associated sphere center than to any other sphere centers. The resulting Voronoi polyhedra are referred to as automaton cells. The average number of Voronoi neighbors of each automaton cell (i.e., the automaton cells that share a common face with

the cell of interest) in our model is 14.8, which is significantly larger than the cell adhesion parameter A_i used in our simulations. In our model, each automaton cell represents either a *single* tumor cell (approximately 15–20 μm in size) or a region of the host microenvironment of similar size. This allows us to explicitly take into account the interactions between a single cell and the surrounding microenvironment. It should be noted that one could also use maximally random jammed sphere packing configurations [47] as a starting point to generate the Voronoi cells. This would result in smaller fluctuations in cell volumes but, for our purposes, this refinement is not necessary.

The heterogeneous host microenvironment of a tumor is composed of various types of stromal cells and the ECM. The ECM is a complex mixture of macromolecules that provides mechanical support for the tissue (such as collagen) and those that play an important role for cell adhesion and motility (such as laminin and fibronectin) [7,48,49]. In the current model, only the effects of the ECM macromolecule density, ECM degradation by the malignant cells, and the pressure due to the ECM deformation on tumor growth are explicitly considered. Henceforth, we will refer to the host microenvironment (or tumor stroma) as the ECM for simplicity. Each ECM-associated automaton cell is assigned a specific density ρ_{ECM}, representing the density of the ECM molecules within the automaton cell. A tumor cell can occupy an ECM-associated automaton cell only if the density of this automaton cell $\rho_{\mathrm{ECM}} = 0$, meaning that the ECM in the automaton cell is either degraded or pushed away by the growing tumor.

A. Cell phenotypes and ECM degradation

Following Ref. [13], the tumor cells consist of two phenotypes: either invasive or noninvasive cells. The noninvasive cells remain in the primary tumor and can be proliferative, quiescent, or necrotic, depending on their nutrient supply. For avascular tumor growth (i.e., no angiogenesis during the growth process), the focus of this paper, the nutrients available to the tumor cells are those that diffuse into the tumor through its surface. As the tumor grows, the amount of nutrient supply, which is proportional to the surface area of the tumor, cannot meet the needs of all cells whose number increases with the tumor volume, leading to the development of necrotic and quiescent regions. The state of a noninvasive cell is determined by its distance to the tumor surface (i.e., the source of nutrients). For example, quiescent cells more than δ_n away from the tumor surface become necrotic (see details in the next section). The effective nutrient diffusion length δ_n (also the characteristic thickness of the rim of living tumor cells) depends on the size of the primary tumor.

As a proliferative cell divides, its daughter cell effectively pushes away or degrades the surrounding ECM and occupies the automaton cell originally associated with the ECM [50–52]. It is easier for a tumor cell to take up an ECM-associated automaton cell with lower density (i.e., soft ECM regions) than that with higher density (i.e., rigid ECM regions) and thus the tumor growth is affected by the ECM heterogeneity through the local mechanical interaction between tumor cells and the ECM. If there is no space available for the placement of a daughter cell within a certain distance from the proliferative cell, the proliferative cell turns quiescent.

The invasive cells are considered to be mutant daughters of the proliferative cells [53], which can gain a variety of degrees of the ECM degradation ability (i.e., the matrix-degradation enzymes) and motility that allow them to leave the primary tumor and invade the surrounding microenvironment [54]. We consider that the invasive cells can move from one automaton cell to another only if the ECM in the target automaton cell is completely degraded (i.e., with $\rho_{\mathrm{ECM}} = 0$). Each attempted move of an invasive cell involves the degradation of the ECM in its neighboring automaton cells, followed by a possible move to one of the automaton cells whose ECM is completely degraded. The nutrient gradient also drives the invasive cells to move as far as possible from the primary tumor [55], which takes up the majority of nutrients. In addition, we assume that the invasive cells do not divide as they migrate.

B. Pressure buildup in confined space

A tumor growing in a confined space compresses the surrounding ECM, which in turn imposes pressure on the tumor [15,50,51]. Following Ref. [14], we explicitly consider the effect of pressure exerted on the growing tumor due to the ECM compression, assuming that the tumor is virtually rigid compared to its ECM [41]. The compressed ECM possesses a larger density, which is assumed to be proportional to the pressure level [14]. It has been shown in Ref. [14] that the probability of division of a tumor cell is reduced by the increase of ECM density due to compression, i.e.,

$$p_{\mathrm{div}} \propto [1 - \omega^*(\xi - 1)], \tag{1}$$

where ω^* is the ECM rigidity parameter proportional to the bulk modulus of the ECM and ξ is the ECM compression parameter, i.e.,

$$\xi = \frac{M - \chi_0 \sum_i^n \rho_{\mathrm{ECM}}(i) v(i)}{V - \sum_i^n v(i)} \frac{V}{M}, \tag{2}$$

where M and V are the initial mass and volume of the ECM, respectively; n is the total number of the ECM-associated automaton cells taken by new tumor cells, $\rho_{\mathrm{ECM}}(i)$ and $v(i)$ are, respectively, the macromolecule density and volume associated with the ith automaton cell, and χ_0 is the ECM degradation ability of the proliferative cells. In other words, Eq. (2) means that the space originally occupied by the ECM macromolecules is taken by the growing tumor and the macromolecules that are not degraded are pushed into a smaller space leading to a higher ECM density (and rigidity). The resulting macromolecule densities in the remaining ECM-associated automaton cells are then given by

$$\rho_{\mathrm{ECM}}(j) = \xi \rho^0_{\mathrm{ECM}}(j) \tag{3}$$

for the jth automaton cell, i.e., the increase of the ECM density after deformation is proportional to its original density. The readers are refereed to Ref. [14] for the derivation and detailed discussion of Eqs. (1)–(3).

C. Tumor-host interface stability

When growing in a rigid microenvironment, a locally smooth tumor surface that results in a huge pressure buildup at the surface is highly undesirable. In contrast, small protrusions on the tumor surface can gain growth advantage by further invading the surrounding ECM to locally release the pressure [20]. These effects are modeled by considering the local geometry of the protrusion tip. Specifically, the width of the tip w is taken to be the linear size of the automaton cell at the protrusion tip. The length of the tip is given by

$$\ell = |\mathbf{x}_c - \mathbf{x}_i| - |\mathbf{x}_c - \bar{\mathbf{x}}|, \tag{4}$$

where $\mathbf{x}_c$ is the geometric center of the tumor, $\mathbf{x}_i$ is the position of the center of the automaton cell at the protrusion tip, and $\bar{\mathbf{x}} = \sum_i^M \mathbf{x}_i/M$ is the average center position of tumor cells neighboring the cell at the protrusion tip. The *growth advantage* gained by the cell at the tip is then proportional to $\xi\ell/w$, which leads to the following probability of division:

$$p_{\rm div} \propto (1 + \xi\ell/w), \tag{5}$$

where ξ is the the ECM-density parameter given by Eq. (2). We note that the quantity ℓ can be either positive or negative, which depends on the radius of curvature at the growth tip.

D. Cell-cell adhesion

In addition to the aforementioned tumor-host interactions that were incorporated in our previous two-dimensional CA models [13,14], we explicitly take into account cell-cell adhesion in the present 3D model. In order for the mutant cells with invasive phenotype to migrate into the surrounding ECM, they first need to detach from the neighboring noninvasive cells in the primary tumor. Strong cell-cell adhesion can prevent the detachment of the mutant cells, which then stay in the primary tumor and undergo the same metabolism cycle as the noninvasive ones.

To explicitly model cell-cell adhesion, we employ a method similar to that used by Anderson [7]: Each mutant cell i has an intrinsic adhesion value A_i, i.e., the minimum number of neighbors of the cell required to keep it attached to the primary tumor. In other words, if the actual number of neighbors A_N is smaller that A_i, the mutant cell can leave the primary tumor. The mutant cells that are unable to detach are treated as proliferative cells. Note that in Ref. [7] a different criterion for cell movement was used. A large value of A_i indicates weak cell-cell adhesion since a large number of neighbors are required to keep the mutant cell in the primary tumor. Similarly, a small value of A_i indicates strong cell-cell adhesion. Although the aforementioned method only provides a somewhat crude modeling of cell-cell adhesion, as shown in Ref. [7] it does capture the salient features of cell adhesion that lead to realistic morphologies of simulated invading tumor.

E. Cellular automaton rules

We now specify the CA rules for our model, which closely follow those given in Refs. [13] and [14], except for the additional rule explicitly incorporating cell-cell adhesion. The values of the parameters used here are chosen such that the CA model can reproduce reported growth dynamics of cultured GBM spheroids from the medical literature [3,27,33]. After generating the automaton cells using Voronoi tessellation, an ECM-density value $\rho_{\rm ECM} \in (0,1)$ is randomly assigned to each automaton cell within a spherical growth-permitting region, which represents the compact space in which the tumor grows. Using random ECM-density values is to account for the heterogeneous host microenvironment. Then a tumor is introduced by designating any one or more of the automaton cells as proliferative cancer cells. Time is then discretized into units that represent one real day. At each time step, the subsequent algorithm is followed.

(i) Each automaton cell is checked for type: invasive, proliferative, quiescent, necrotic, or ECM associated. Invasive cells degrade and migrate into the ECM surrounding the growing tumor. Proliferative cells are actively dividing cancer cells, quiescent cancer cells are those that are alive, but do not have enough nutrients to support cellular division, and necrotic cells are dead cancer cells.

(ii) All tumorous necrotic cells are inert (i.e., they do not change type).

(iii) Quiescent cells more than a certain distance δ_n from the tumor's edge are turned necrotic. The tumor's edge, which is assumed to be the source of oxygen and nutrients, consists of all ECM-associated automaton cells that border the neoplasm. The critical distance δ_n for quiescent cells to turn necrotic is computed as follows:

$$\delta_n = a L_t^{(d-1)/d}, \tag{6}$$

where $a = 0.58\ \text{mm}^{1/2}$ is the base necrotic thickness controlled by nutritional needs, d is the Euclidean spatial dimension, and L_t is the distance between the geometric centroid $\mathbf{x}_c$ of the tumor (i.e., $\mathbf{x}_c = \sum_i^N \mathbf{x}_i/N$, where N is the total number of cells in the tumor) and the tumor edge cell that is closest to the quiescent cell under consideration.

(iv) A proliferative cell will divide if there is space available for the placement of a daughter cell within a distance δ_p from the proliferative cell, which is given by

$$\delta_p = b L_t^{(d-1)/d},$$

where $b = 0.30\ \text{mm}^{1/2}$ is the base proliferative thickness controlled by nutritional needs, d is the spatial dimension, and L_t is the distance between the geometric tumor centroid $\mathbf{x}_c$ and the tumor edge cell that is closest to the proliferative cell under consideration. As discussed in the previous section, we consider that the probability of division $p_{\rm div}$ for a specific proliferative cell depends on the local ECM density [13,14], the pressure imposed by the ECM [Eq. (1)], and the local geometry of the tumor-host interface [Eq. (5)], i.e.,

$$p_{\rm div} = p_0[1 - \rho_{\rm ECM} - \omega^*(\xi - 1) + \xi\ell/w], \tag{7}$$

where $p_0 = 0.192$ is the base probability of division linked to cell-doubling time, $\rho_{\rm ECM}$ is the local ECM density, $\omega^* = 2\rho_{\rm ECM}^0$ is a parameter taking into account the effect of pressure [14], ξ is the ratio of current average ECM density over the initial density defined by Eq. (2), and ℓ and w are, respectively, the length and width of local protrusion tips. A proliferative cell turns quiescent if there is no space available for the placement of a daughter cell within a distance δ_p from the proliferative cell.

(v) If a proliferative cell divides, it can produce a mutant daughter cell possessing an invasive phenotype with a prescribed probability $\gamma = 0.05$ (i.e., the mutation rate). The invasive daughter cell gains ECM degradation ability $\chi_1 = 0.95$ and motility $\mu = 2$ (i.e., the maximum number of "jumps" made by an invasive cell from one automaton cell to another per day), which enables it to leave the primary tumor and invade the surrounding ECM. The rules for updating mutant cells are given in steps (vi) and (vii). If the daughter cell is noninvasive, it is designated as a new proliferative cell.

(vi) Each mutant cell i with invasive phenotype is assigned an adhesion value $A_i \in [2,8]$ (i.e., the minimum number of neighbors required for attachment of an invasive cell to the primary tumor). If the adhesion value is greater than the number A_N of noninvasive neighbor cells (whose automaton cells share a face with that of the mutant cell), i.e., $A_i \geqslant A_N$, the mutant cell is designated as an invasive cell. Otherwise, it is designated as a proliferative cell.

(vii) An invasive cell degrades the surrounding ECM (i.e., those in the neighboring automaton cells of the invasive cell) and can move from one automaton cell to another if the associated ECM is completely degraded locally. For an invasive cell with motility μ and ECM degradation ability χ_1, it will make m attempts to degrade the ECM in the neighboring automaton cells and jump to these automaton cells, where m is an arbitrary integer in $[0,\mu]$. For each attempt, the surrounding ECM density ρ_{ECM} is decreased by $\delta\rho$, where $\delta\rho$ is an arbitrary number in $[0,\chi_1]$. Using random numbers for the ECM degradation ability and cellular motility is to represent the stochasticity of the invasion process. If more than one neighboring automaton cell of the invasive cell is completely degraded (i.e., $\rho_{\mathrm{ECM}} = 0$), the invasive cell moves in a direction that maximizes its nutrient and oxygen supply. Here we assume that the migrating invasive cells *do not divide*. The degraded ECM shows the invasive path of the tumor.

(viii) The density ρ_{ECM} of the remaining ECM automaton cells is updated according to Eq. (3).

We note that although only spherical growth-permitting regions are considered here, this constraint can be easily relaxed to other shapes. In this paper, we will mainly employ the CA model to investigate the growth dynamics and morphologies of the malignant tumors in three dimensions. However, the algorithmic details of the model and the CA rules are presented for any spatial dimension and the model can be easily implemented in two dimensions as well.

III. RESULTS

In this section, we apply the CA model to investigate systematically microenvironment-enhanced invasive behavior of malignant tumors in three dimensions, which is computationally more extensive than our previous studies in two dimensions [13,14]. Specifically, simulating the growth of a 2D tumor from a few cells to a macroscopic-size tumor with $\sim 10^4$ cells only takes a few minutes on a standard Dell Workstation (Precision T3400), while the simulation of the growth of a 3D tumor to macroscopic size ($\sim 10^6$ cells) can take up to a few hours. Given accurate knowledge of the microenvironment in which the tumor grows, the 3D model in principle enables one to obtain realistic morphologies of both the primary tumor and invasive branches, which are crucial to the diagnosis, prognosis, and treatment of the tumor.

To correctly capture the salient features of invasive growth, such as the emergence of long dendritic invasive branches, the growth-permitting region should contain at least $\sim 1\,000\,000$ automaton cells, representing a tissue of size ~ 1 mm^3. Initially, a small subset of the automaton cells ($N \sim 100$) at the center of the growth-permitting region are designated as proliferative cells. Then the initial tumor is allowed to grow according to the CA rules. Statistics of the tumor (e.g., volume, radius, and number of cells of different types) and its morphology (i.e., the geometrical positions of the tumor cells and the degraded ECM associated cells) are collected every T_c days. The statistics reported here are averaged over ten independent simulations for each case.

The ECM density value is randomly assigned in order to represent the heterogeneous microenvironment in which the tumor grows [13,14], i.e., $\rho^i_{\mathrm{ECM}} = 2\bar{\rho}_{\mathrm{ECM}} z$, where z is a random number in $[0, 1]$ and $\bar{\rho}_{\mathrm{ECM}}$ is a prescribed average ECM density. In addition, we consider that a growing tumor can continuously receive nutrients from the boundary of the growth-permitting region. In the simulations that follow, we consider a constant radially symmetric nutrient gradient in the growth-permitting region with the highest nutrient concentration at the vascular boundary. We note that although generally the nutrient concentration field *in vivo* is more complex, previous numerical studies that considered the exact spatial-temporal evolution of the nutrient concentration field

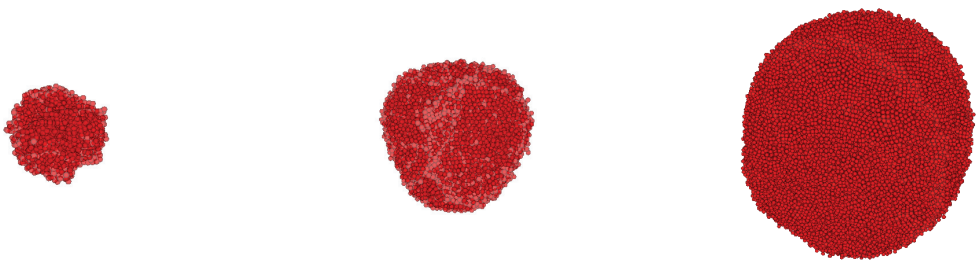

(a) Day 20 (b) Day 60 (c) Day 100

FIG. 2. (Color online) Snapshots of a 3D proliferative tumor growing in a soft ECM with $\bar{\rho}_{\mathrm{ECM}} = 0.15$.

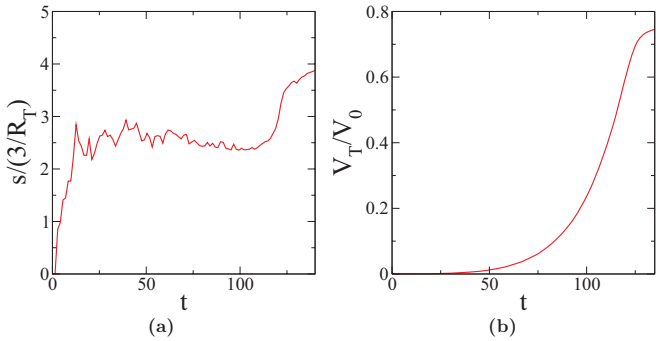

FIG. 3. (Color online) Statistics of the 3D proliferative tumor growing in the soft ECM with $\bar{\rho}_{\mathrm{ECM}} = 0.15$ shown in Fig. 2. (a) Scaled specific surface versus time, where R_T is the effective radius of tumor. (b) Tumor volume V_T normalized by the volume V_0 of the growth-permitting region versus time.

have shown a decay of the concentrations toward the tumor center [7,8], for which our constant-gradient approximation is a very reasonable one.

The specific surface s, defined as the ratio of the surface area of the primary tumor over its total volume [46], is employed to characterize the roughness or degree of "fingering" at the surface [13,14] of the primary tumor. In particular, the deviation of the specific surface of a tumor from that of a sphere $3/R$ (where R is the radius of the sphere) provides a roughness measurement. If the deviation is small, the tumor possesses a smooth spherelike shape. Otherwise, the tumor is considered to have a rough surface. Therefore, the scaled specific surface $s/(3/R_T)$ is used here for an arbitrary-shaped tumor with an effective radius R_T (i.e., the average distance from tumor edge to tumor center). Moreover, the volume of the tumor V_T is normalized with respect to that of the growth permitting region V_0.

In the visualizations of the 3D tumors that follow, we only show the outer most proliferative cells in the primary tumor [red (dark gray in print version)] and the invasive branches [blue (light gray in print version)] composed of automaton cells associated with the ECM degraded by the invasive cells. Note that unlike the visualization of 2D tumors [13,14] in which necrotic, quiescent, and invasive cells can all be clearly shown, it is difficult to render a clear 3D visualization with these cells simultaneously shown. Instead, quantitative statistics of these cells (i.e., cell number as a function of time) are given.

A. Proliferative tumors

To validate our CA model, we first consider the growth of a proliferative (noninvasive) tumor in confined space with a soft ECM, a case that has been extensively investigated [26–29,32–41]. It is well established that such a growth is characterized by the Gompertz dynamics: Growth rate is initially slow, then exponentially increases at intermediate times, and finally plateaus at large times [27].

Figure 2 shows the snapshots of the simulated tumor growing in a soft ECM with $\bar{\rho}_{\mathrm{ECM}} = 0.15$. It can be clearly seen that the tumor develops spherelike shape, which is also indicated by the small values of the scaled specific surface [see Fig. 3(a)]. The tumor volume (proportional to the total number of cells in the tumor) as a function of time is shown in Fig. 3(b), indicating the Gompertzian growth of the tumor [27]. We note that the values of the parameters used are chosen such that the CA model can reproduce reported growth dynamics of GBM from the medical literature [3,27,33]. In the later growth stages, due to the significant compression of the ECM by the tumor, a high pressure is inevitably built up even though the ECM is very soft initially. This results in a bumpy tumor surface to release the high pressure locally, as indicated by the increase of the scaled specific surface [see Fig. 3(a)].

We now consider a tumor growing in a rigid ECM with $\bar{\rho}_{\mathrm{ECM}} = 0.65$. As discussed in Sec. II B, the compression of the rigid ECM due to the growth of the tumor results in a high pressure exerted on the tumor. Thus the tumor surface is unstable with respect to local protrusions, which can gain growth advantage by further reaching out into the distant ECM to release local pressure. Indeed, as shown in Fig. 4, fingerlike protrusions on the tumor surface emerge at early growth stages and no spherical tumor shape is observed. The associated scaled specific surface $s/(3/R_T)$ monotonically increases as the tumor grows. This results from the emergence of protrusions, which is an indication of the instability of the tumor surface [see Fig. 5(a)].

Although the actual volume of the tumor growing in the rigid ECM is significantly smaller than the tumor growing in the soft ECM on the same day of growth [see Fig. 5(b)], its effective size (e.g., the volume of the smallest sphere that completely inscribes the tumor) is comparable to the tumor in the soft ECM (see Figs. 4 and 2). In addition, it can be seen from Fig. 5(b) that the tumor in the rigid ECM is still in the linear growth regime by the end of our simulation (i.e., day 120 of growth), while the tumor in the soft ECM has reached its

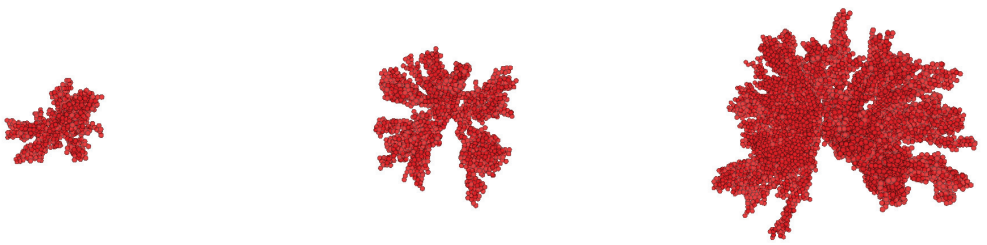

(a) Day 20 (b) Day 60 (c) Day 100

FIG. 4. (Color online) Snapshots of a 3D proliferative tumor growing in a rigid ECM with $\bar{\rho}_{\mathrm{ECM}} = 0.65$.

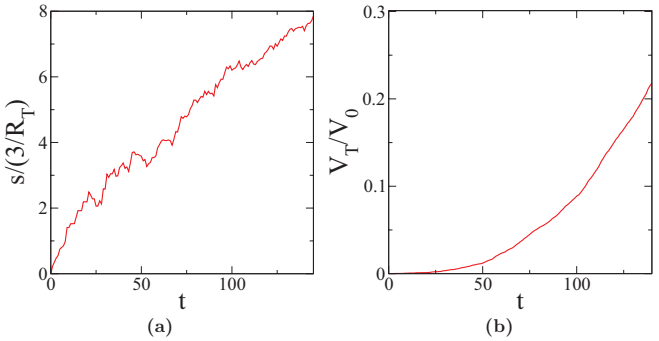

FIG. 5. (Color online) Statistics of the 3D proliferative tumor growing in the rigid ECM with $\bar{\rho}_{\mathrm{ECM}} = 0.65$ shown in Fig. 4. (a) Scaled specific surface versus time, where R_T is the effective radius of tumor. (b) Tumor volume V_T normalized by the volume V_0 of the growth-permitting region versus time.

plateau size. This suggests that the tumor in a rigid ECM (i.e., a harsh microenvironment) can have a much larger effective size than the tumor in a soft ECM, which significantly increases its malignancy.

B. Invasive tumors: ECM rigidity vs cell-cell adhesion

In this section, we consider the growth of invasive tumors with mutant daughter cells detaching from the primary tumor and migrate into the surrounding ECM. Specifically, we focus on the effects of ECM rigidity (i.e., the harshness of the microenvironment) and cell-cell adhesion on the growth dynamics and morphology of the tumor. We note that the effects of cell-cell adhesion were not explicitly considered in our previous two-dimensional CA models [13,14].

Again, we first consider tumors growing in a soft ECM with $\bar{\rho}_{\mathrm{ECM}} = 0.15$. In the case of weak cell-cell adhesion (i.e., $A_i = 8$), the primary tumor possesses a smooth and compact shape (see Fig. 6). Recall that A_i is the minimum number of neighbors required for keeping the mutant cell i with invasive phenotype remaining in the primary tumor. Thus a large value of A_i indicates weak cell-cell adhesion since a large number of neighbors are required to keep the mutant cell attached to the primary tumor. The tumors possess linearlike elongated invasive branches emanating from the primary tumor, which are evenly distributed over the tumor surface. In the case of strong cell-cell adhesion (i.e., $A_i = 2$), the number of invasive branches is significantly reduced (Fig. 7). Although the same mutation rate is used for both cases, due to strong cell-cell adhesion, the number of mutant cells that actually detach from the primary and invade the surrounding ECM is much smaller, as can be seen in Figs. 6(d) and 7(d). This suggests that strong cell-cell adhesion can reduce the malignancy of invasive tumors growing in a soft ECM.

As shown in the previous section, tumors growing in the rigid ECM with $\bar{\rho}_{\mathrm{ECM}} = 0.65$ develop fingerlike protrusions on the primary tumor surface to locally release the high pressure exerted by the compressed ECM. The cells at the tips of these protrusions usually have a small number of neighbors and thus are easier to detach from the primary tumor. Figures 8 and 9 respectively show snapshots of invasive tumors with weak ($A_i = 8$) and strong ($A_i = 2$) cell-cell adhesion in a rigid ECM and the associated statistics of the number of tumor cells of different type. It can be seen that linearlike extended invasive branches emanate from the tips of the protrusions on the tumor surface. It is clear from both the snapshots and statistics that the degree of invasion (e.g., the number of the invasive branches and invasive cells) has not been significantly affected by the strength of cell adhesion. In other words, even in the case of strong cell-cell adhesion, the invasive behavior is still prominent, in contrast to the tumors growing in a soft ECM. This implies that harsh microenvironments can significantly enhance the malignant behavior of invasive tumors.

C. Phase diagram for tumor-malignancy behaviors

Our simulations indicate that while increasing ECM rigidity enhances malignancy, increasing cell-cell adhesion acts conversely. The competition between these two different malignancy mechanisms results in a qualitative phase diagram characterizing the malignant behavior of the invasive solid tumor (see Fig. 10). The vertical axis of the phase diagram represents the rigidity of the ECM (i.e., harshness of the microenvironment) and the horizontal axis represents the strength of the cell-cell adhesion. The solid curve separates invasive and noninvasive behaviors. Hence, crossing this boundary

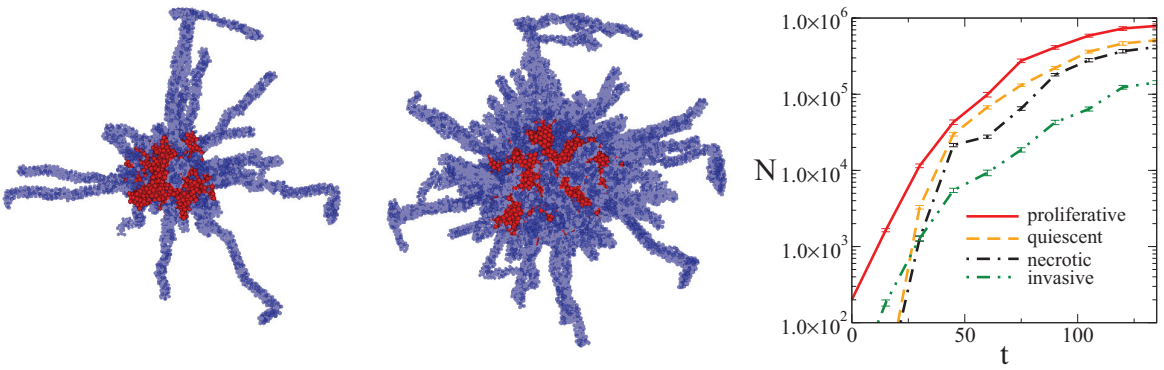

FIG. 6. (Color online) (a) and (b) Snapshots of a 3D invasive tumor with weak cell-cell adhesion ($A_i = 8$) growing in a soft ECM with $\bar{\rho}_{\mathrm{ECM}} = 0.15$. Linear-like extended invasive branches emanate from the primary tumor, which are evenly distributed over the tumor surface. (c) Statistics of the number of different cells as a function of time.

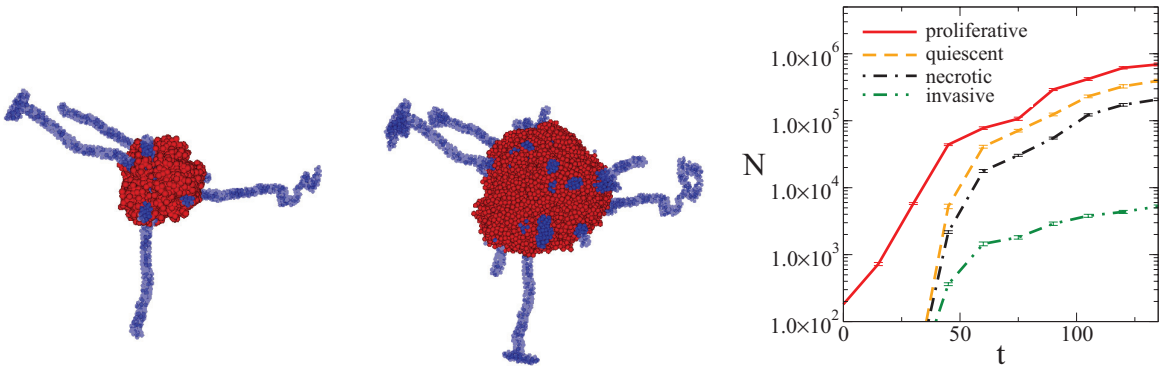

(a) Day 50 (b) Day 80 (c)

FIG. 7. (Color online) (a) and (b) Snapshots of a 3D invasive tumor with strong cell-cell adhesion ($A_i = 2$) growing in a soft ECM with $\bar{\rho}_{\mathrm{ECM}} = 0.15$. The number of the invasive branches emanating from the primary tumor is much smaller than that for tumors with weak cell-cell adhesion (see Fig. 6). (c) Statistics of the number of different cells as a function of time.

constitutes a noninvasive-invasive phase transition [25], analogous to those that occur in many-particle systems [46].

We have found that for very weak cell adhesion, any mutant cell with an invasive phenotype can leave the primary tumor and invade the surrounding ECM despite the ECM rigidity level. This corresponds to the low-adhesion-invasive regime (i.e., the left part of diagram) in which no transition from noninvasive behavior to invasive behavior occurs. As the strength of cell adhesion increases, our simulations indicate that only cells with a small number of contacting neighbors (i.e., the cells at the tips of fingerlike protrusion on the tumor surface) can detach from the primary tumor. The transition from noninvasive behavior to invasive behavior in this intermediate-adhesion regime (i.e., the middle part of the diagram) is very sensitive to the ECM rigidity. In the case of very strong cell-cell adhesion, the invasive behavior becomes less sensitive to the ECM rigidity but is still enhanced by it. This corresponds to the high-adhesion regime (i.e., the right part of the diagram).

A tumor with a specific cell-cell adhesion strength growing in a confined soft microenvironment can be noninvasive initially. As the tumor grows in volume, it compresses the surrounding ECM, which makes the microenvironment increasingly more rigid. This phenomenon eventually would induce invasive behavior. The aforementioned process corresponds to a vertical line in the phase diagram, which starts from the noninvasive regime and eventually crosses into the invasive regime.

Finally, we would like to note that the 3D CA model in its current implementation only allows us to explore a limited range of the parameters for the phase diagram. For example, one can expect in principal a threshold for invasiveness at very high ECM rigidity. This would result in a more complex phase diagram than the one shown here.

IV. CONCLUSIONS AND DISCUSSION

In this paper, we generalized a recently developed two-dimensional cellular automaton model to investigate the microenvironment-enhanced malignant behavior of avascular invasive solid tumors in three dimensions. Our CA model incorporates a variety of microscopic-scale tumor-host interactions, including the degradation of the ECM by the malignant cells, nutrient-driven cell migration, pressure buildup due to the compression of the ECM, and its effect on the local tumor-host interface stability. Moreover, in the present work, unlike Refs. [13] and [14], we explicitly considered the effects of cell-cell adhesion on the growth dynamics of invasive

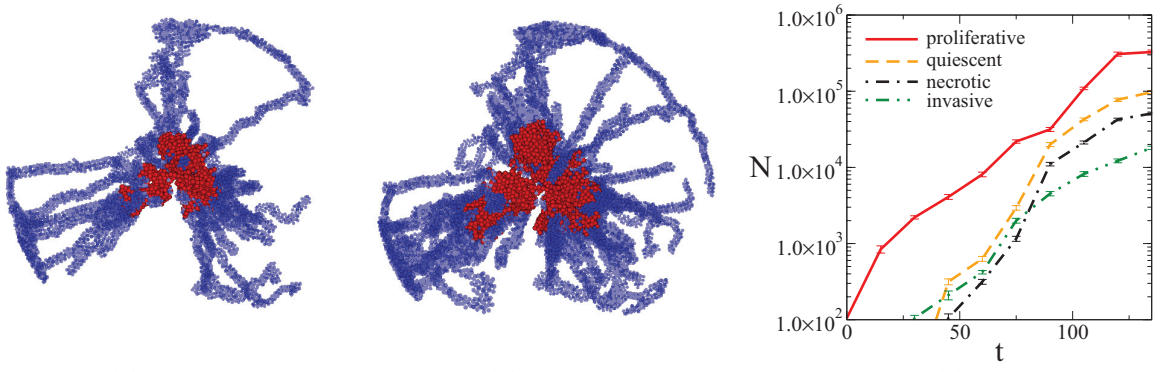

(a) Day 50 (b) Day 80 (c)

FIG. 8. (Color online) (a) and (b) Snapshots of a 3D invasive tumor with weak cell-cell adhesion ($A_i = 8$) growing in a rigid ECM with $\bar{\rho}_{\mathrm{ECM}} = 0.65$. Linearlike extended invasive branches emanate from the tips of the protrusions on the tumor surface [56]. (c) Statistics of the number of different cells as a function of time.

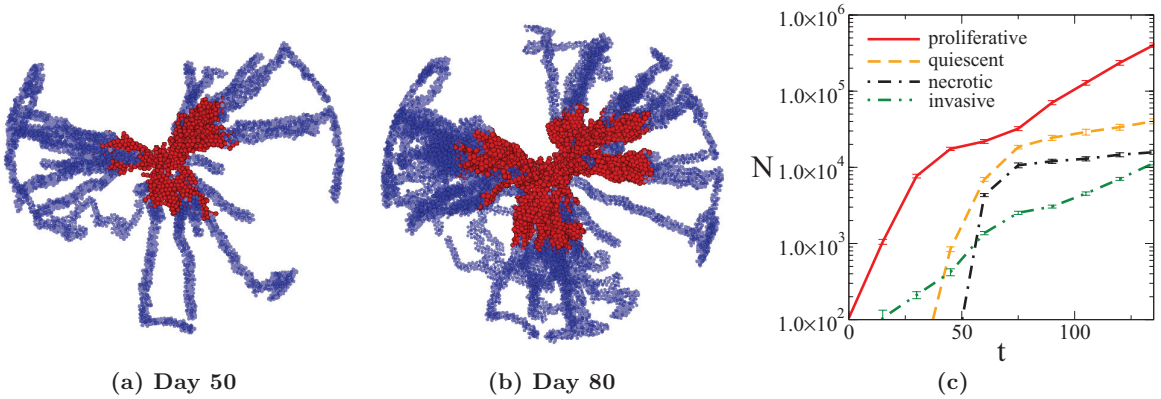

(a) Day 50 (b) Day 80 (c)

FIG. 9. (Color online) (a) and (b) Snapshots of a 3D invasive tumor with strong cell-cell adhesion ($A_i = 2$) growing in a rigid ECM with $\bar{\rho}_{\mathrm{ECM}} = 0.65$. The number of the invasive branches emanating from the tips of the protrusions [56] on the tumor surface is comparable to that for tumors with weak cell-cell adhesion (see Fig. 8). (c) Statistics of the number of different cells as a function of time.

tumors. We find that while strong cell-cell adhesion can suppress the invasive behavior of the tumors growing in a soft ECM, tumor malignancy can be significantly enhanced by the rigidity of the ECM resulting in fingerlike protrusions on the surface of the primary tumor, which facilitate the detaching of mutant invasive cells. Our results emphasize the importance of understanding the complex tumor-host interactions in both fundamental cancer research and clinical treatment.

Moreover, we inferred from our simulation results a qualitative phase diagram to characterize malignancy in terms of two competing effects: rigidity of the ECM and cell-cell adhesion. We found that as a tumor grows in a confined microenvironment (a common situation for the majority of solid tumors *in vivo*), it is inevitable that a high pressure will be built even the ECM is initially soft. Thus a tumor with a low level of malignancy initially can eventually develop highly malignant invasive behavior. This suggests that by properly tuning the microenvironmental parameters, it would be possible to keep the tumor in the less malignant noninvasive phase. Thus treatments that target the host microenvironment instead of the neoplasm itself might be profitable.

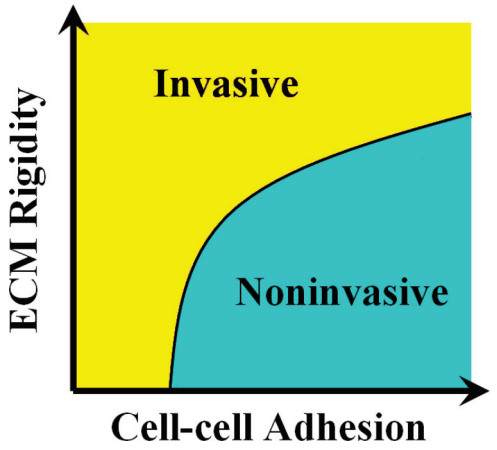

FIG. 10. (Color online) Schematic phase diagram inferred from the simulation results that characterizes malignant behaviors of invasive tumors. The vertical axis represents the rigidity of the ECM (i.e., harshness of the microenvironment) and the horizontal axis represents the strength of cell-cell adhesion. While tumor malignancy is enhanced by higher ECM rigidity, it is reduced by stronger cell-cell adhesion. The competition between these two effects results in the solid curve in the diagram that separates invasive and noninvasive behaviors.

Although as currently implemented our CA model is readily applied to characterize *in vitro* tumor growth, we expect that the conclusions drawn here still qualitatively apply to *in vivo* situations. More realistic microenvironments including heterogeneities such as fibroblasts, blood vessels, and lymphatics, which play an important role in clinical cancers, as well as other relevant mechanisms (e.g., tumor and normal cell phenotypic plasticity and immune response) should be properly incorporated in the model in order to attempt to provide qualitatively predictions for clinical cancer progression. Specifically, such a realistic model would enable one to render virtual 3D tumor morphology that statistically represents the spatial organization of tumor cells observed in the histological slices of the tumor [57], which could lead to more accurate diagnosis and thus more effective tumor treatment strategies. The development of microscopic models to quantify the transport and mechanical properties of the extracellular matrix [58] is an important avenue for cancer research in light of the ECM's key role in the transmission of biomechanical or biochemical cues and the regulation of cell motility, proliferation, differentiation, and apoptosis. In addition, realistic and robust tumor models will enable one to efficiently design, test, and optimize tumor treatments [29,59–61].

ACKNOWLEDGMENTS

The authors thank Duyu Chen for valuable discussions and suggestions. The authors are also grateful to an anonymous reviewer for thoughtful comments. The research described was supported by the National Cancer Institute under Award No. U54CA143803. The content is solely the responsibility of the authors and does not necessarily represent the official views of the National Cancer Institute or the National Institutes of Health. S.T. thanks the Department of Physics and Astronomy at the University of Pennsylvania for their hospitality during his stay there.

[1] D. S. Coffey, Nat. Med. **4**, 882 (1998).
[2] D. Hanahan and R. A. Weinberg, Cell **100**, 57 (2000).
[3] T. S. Deisboeck, M. E. Berens, A. R. Kansal, S. Torquato, A. Rachamimov, D. N. Louis, and E. A. Chiocca, Cell Proliferat. **34**, 115 (2001).
[4] I. J. Fidler, Nat. Rev. Cancer **3**, 453 (2003).
[5] R. S. Kerbel, Adv. Cancer Res. **55**, 87 (1990).
[6] L. A. Liotta and E. C. Kohn, Nat. Genet. **33**, 10 (2003).
[7] A. R. A. Anderson, Math. Med. Biol. **22**, 163 (2005).
[8] A. R. A. Anderson, A. M. Weaver, P. T. Cummings, and V. Quaranta, Cell **127**, 905 (2005).
[9] H. B. Frieboes, X. M. Zheng, C. H. Sun, B. Tromberg, R. A. Gatenby, and V. Gristini, Cancer Res. **66**, 1597 (2006).
[10] Z. J. Chen, G. T. Gillies, W. C. Broaddus, S. S. Prabhu, H. Fillmore, R. M. Mitchell, F. D. Corwin, and P. P. Fatouros, J. Neurosurg. **101**, 314 (2004).
[11] R. A. Gatenby, Eur. J. Cancer **32**, 722 (1996).
[12] E. R. Fearon and B. Vogelstein, Cell **61**, 759 (1990).
[13] Y. Jiao and S. Torquato, PLoS Comput. Biol. **7**, e1002314 (2011).
[14] Y. Jiao and S. Torquato, AIP Adv. **2**, 011003 (2012).
[15] G. Helmlinger, P. A. Netti, H. C. Lichtenbeld, R. J. Melder, and R. K. Jain, Nat. Biotechnol. **15**, 778 (1997).
[16] M. C. Hogan, A. Lee, L. A. Solberg, and S. D. Thome, Am. J. Hematol. **70**, 55 (2002).
[17] T. P. Padera, A. Kadambi, E. di Tomaso, C. M. Carreira, E. B. Brown, Y. Boucher, N. C. Choi, D. Mathisen, J. Wain, E. J. Mark *et al.*, Science **296**, 1883 (2002).
[18] A. Bru and D. Casero, J. Theor. Biol. **243**, 171 (2006).
[19] M. J. Paszek, N. Zahir, K. R. Johnson, J. N. Lakins, G. I. Rozenberg, A. Gefen, C. A. Reinhart-King, S. S. Margulies, M. Dembo, D. Boettiger *et al.*, Cancer Cell **8**, 241 (2005).
[20] C. Guiot, N. Pugno, P. P. Delsanto, and T. S. Deisboeck, Phys. Biol. **4**, P1 (2007).
[21] R. A. Gatenby and P. K. Maini, Nature (London) **421**, 321 (2003).
[22] H. M. Byrne, T. Alarcon, M. R. Owen, S. D. Webb, and P. K. Maini, Philos. Trans. R. Soc. Ser. A **364**, 1563 (2006).
[23] A. R. A. Anderson and V. Quaranta, Nat. Rev. Cancer **8**, 227 (2008).
[24] H. M. Byrne, Nat. Rev. Cancer **10**, 221 (2010).
[25] S. Torquato, Phys. Biol. **8**, 015017 (2011).
[26] A. R. A. Anderson and M. A. J. Chaplain, Bull. Math. Biol. **60**, 857 (1998).
[27] A. R. Kansal, S. Torquato, G. R. Harsh, E. A. Chiocca, and T. S. Deisboeck, J. Theor. Biol. **203**, 367 (2000).
[28] A. R. Kansal, S. Torquato, E. A. Chiocca, and T. S. Deisboeck, J. Theor. Biol. **207**, 431 (2000).
[29] J. E. Schmitz, A. R. Kansal, and S. Torquato, J. Theor. Med. **4**, 223 (2002).
[30] T. Alarcon, H. M. Byrne, and P. K. Maini, J. Theor. Biol. **229**, 395 (2004).
[31] D. J. Gavaghan, J. M. Brady, C. P. Behrenbruch, R. P. Highnam, and P. K. Maini, J. Theor. Med. **4**, 3 (2002).
[32] J. L. Gevertz and S. Torquato, J. Theor. Biol. **243**, 517 (2006).
[33] J. L. Gevertz, G. T. Gillies, and S. Torquato, Phys. Biol. **5**, 036010 (2008).
[34] J. L. Gevertz and S. Torquato, Phys. Rev. E **80**, 051910 (2009).
[35] N. Bellomo and L. Preziosi, Math. Comput. Model **32**, 413 (2000).
[36] M. Scalerandi, B. C. Sansone, and C. A. Condat, Phys. Rev. E **65**, 011902 (2001).
[37] M. Scalerandi and B. C. Sansone, Phys. Rev. Lett. **89**, 218101 (2002).
[38] Y. Kim and A. Friedman, Bull. Math. Biol. **72**, 1029 (2010).
[39] D. L. McElwain and G. J. Pettet, Bull. Math. Biol. **55**, 655 (1993).
[40] C. Y. Chen, M. Byrne, and J. R. King, J. Math. Biol. **43**, 191 (2001).
[41] T. Roose, P. Netti, L. Munn, Y. Boucher, and R. Jain, Microvasc. Res. **66**, 204 (2003).
[42] R. A. Gatenby and E. T. Gawlinski, Cancer Res. **56**, 5745 (1996).
[43] R. A. Gatenby, E. T. Gawlinski, A. F. Gmitro, B. Kaylor, and R. J. Gillies, Cancer Res. **66**, 5216 (2006).
[44] P. Macklin and J. Lowengrub, J. Theor. Biol. **245**, 677 (2007).
[45] A. Gerisch and M. A. J. Chaplain, J. Theor. Biol. **250**, 684 (2008).
[46] S. Torquato, *Random Heterogeneous Materials: Microstructure and Macroscopic Properties* (Springer, New York, 2002).
[47] S. Torquato and F. H. Stillinger, Rev. Mod. Phys. **82**, 2633 (2010); S. Torquato and Y. Jiao, Phys. Rev. E **82**, 061302 (2010).
[48] J. L. Gevertz and S. Torquato, PLoS Comput. Biol. **4**, e1000152 (2008).
[49] K. Burridge and M. Chrzanowska-Wodnicka, Annu. Rev. Cell Dev. Biol. **12**, 463 (1996).
[50] M. Sarntinoranont, F. Rooney, and M. Ferrari, Ann. Biomed. Eng. **31**, 327 (2003).
[51] V. D. Gordon, M. T. Valentine, M. L. Gardel, D. Andor-Ardo, S. Dennison, A. A. Bogdanov, D. A. Weitz, and T. S. Deisboeck, Exp. Cell Res. **289**, 58 (2003).
[52] L. A. Liotta, C. N. Rao, and S. H. Barsky, Lab. Invest. **49**, 636 (1983).
[53] J. O. Boyle, J. Hakim, and W. Koch, Cancer Res. **53**, 4477 (1993).
[54] W. G. Stetler-Stevenson, S. Aznavoorian, and L. A. Liotta, Annu. Rev. Cell Biol. **9**, 541 (1993).
[55] J. A. Lawrence and P. S. Steeg, World J. Urol. **14**, 124 (1996).
[56] Although it might be difficult to clearly see from the snapshots of the 3D tumor morphology that invasive branches emanate from the protrusion tips at the tumor surface, we reached this conclusion by carefully examining and rotating an interactive 3D model of the tumor.
[57] Y. Jiao, H. Berman, T.-R. Kiehl, and S. Torquato, PLoS ONE **6**, e27323 (2011).
[58] Y. Jiao and S. Torquato, Phys. Biol. **9**, 036009 (2012).
[59] J. L. Gevertz, Comput. Math. Methods Med. **2011**, 830515 (2011).
[60] J. L. Gevertz, Phys. Rev. E **85**, 041914 (2012).
[61] H. Enderling, M. A. J. Chaplain, A. R. A. Anderson, and J. Vaidya, J. Theor. Biol. **246**, 245 (2007).